Journal of Materials Chemistry

www.rsc.org/materials

Volume 20 | Number 38 | 14 October 2010 | Pages 8175–8418

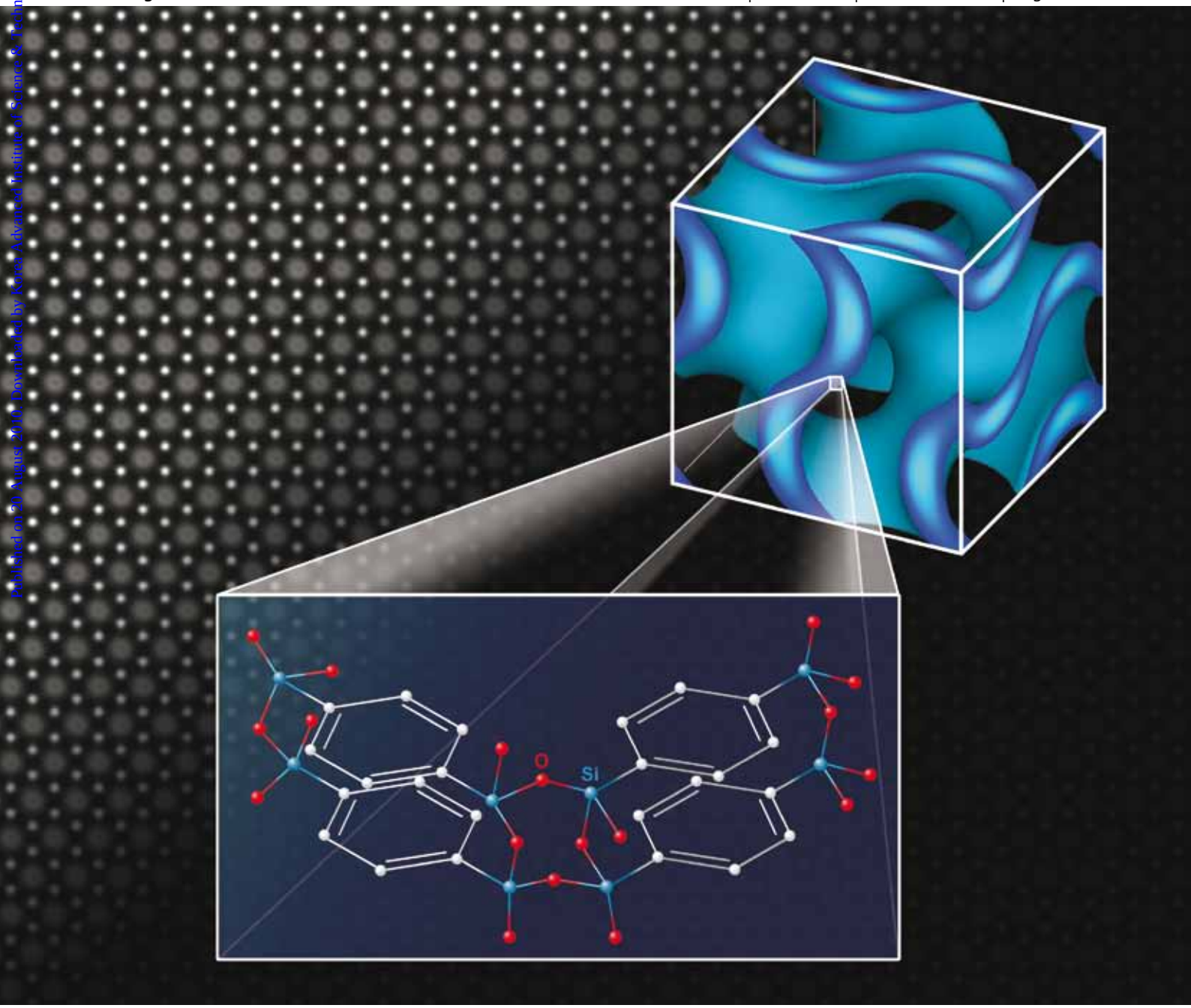

ISSN 0959-9428

RSC Publishing

Large pore phenylene-bridged mesoporous organosilica with bicontinuous cubic *Ia*$\bar{3}$*d* (KIT-6) mesostructure†

Wanping Guo,[a] Freddy Kleitz,[c] Kanghee Cho[ab] and Ryong Ryoo*[ab]

Received 19th May 2010, Accepted 27th June 2010
DOI: 10.1039/c0jm01518k

Assembly of mesostructured silica using Pluronic P123 triblock copolymer (EO_{20}-PO_{70}-EO_{20}) and n-butanol is a facile synthesis route to the MCM-48-like ordered large mesoporous silicas with the cubic *Ia*$\bar{3}$*d* mesostructure, which are designated KIT-6. This synthesis route has been successfully extended to phenylene-bridged organosilicas from the limit so far for silica, using 1,4-bis(triethoxysilyl)benzene as an organosilica source and re-optimizing the synthesis conditions. In particular, optimal acid concentration and reagent ratios were determined to allow facile synthesis of the bicontinuous cubic mesophase in high yield and high phase purity. The products were characterized by powder X-ray diffraction (XRD), transmission electron microscopy, solid state NMR spectroscopy and analysis of nitrogen sorption at −196 °C using modern non-local density functional theory methods. This synthesis procedure enabled easy fine tuning of pore volume, specific surface area and mesopore size by variation of the hydrothermal aging temperature between 80 and 130 °C. Furthermore, wide angle XRD data suggest short range molecular-scale periodicity in the framework walls originating from regular arrangement of the bridging aromatic groups. These KIT-6 organosilica materials with fully interconnected nanoporous structure would be readily available for applications in heterogeneous catalysis, selective adsorption, and nanostructure design *via* solid templating approaches.

Introduction

The three-dimensional (3-D) cubic mesoporous material designated KIT-6[1–3] is a large pore mesostructured silica (pore size > 5 nm) which consists of two continuous and interpenetrating systems of chiral channels, producing an intricately interwoven 3D network of cylindrical-like open mesopores with a structure commensurate with the *Ia*$\bar{3}$*d* symmetry. Mesoporous KIT-6 silica is now attracting wide interest owing to the great perspectives of application of such a fully interconnected nanoporous structure in catalysis,[4] adsorption and separation,[5] and nanostructure design through solid templating approaches.[6] Indeed, this unique 3-D interconnected network provides a highly open porous host with an easy and direct access for guest species, thus facilitating inclusion or diffusion throughout the pore system without pore blockage. With this regard, evidence for enhanced diffusion properties in 3-D cubic *Ia*$\bar{3}$*d* mesostructured porous materials as compared to other pore network geometries have recently been provided.[7,8]

The synthesis of purely siliceous KIT-6 is rather straightforward and highly reproducible based on the use of a mixture of n-butanol and triblock copolymer P123 ($EO_{20}PO_{70}EO_{20}$) as structure-directing agents under moderately acidic aqueous conditions (*e.g.*, 0.3–0.75 M).[1,3] Furthermore, it was demonstrated that a prolonged hydrothermal treatment at high temperatures of the thus-obtained silica powder (≥ 100 °C) leads to a totally interconnected continuous pore system whereas an aging performed at temperatures below 80 °C usually results in the two sub-networks of mesopores remaining isolated from each other.[3,9–11] Thus, under given synthesis conditions, a fully continuous 3-D pore system can be generated with the silica walls following the gyroid (G) infinite periodic minimal surface (IPMS).[12–15] On the other hand, the synthesis of a large pore periodic mesoporous organosilica (PMO) analogue of the KIT-6 silica still remains challenging.

PMOs are mesoporous organic-inorganic hybrids synthesized from bridged bis-silsesquioxane precursors (*e.g.*, $(R'O)_3Si$-R-$Si(OR')_3$ with $R' = CH_3$ or C_2H_5 and R = alkyl-, allyl-, aryl, *etc.*) in the presence of surfactant amphiphiles following cooperative self-assembly principles.[16–23] In particular, PMOs are characterized by uniform distributions of organic groups inside of their framework walls, thus resulting in mesoporous materials with high-loading of organic functions with no pore blockage. Furthermore, the chemical and physical properties of PMOs can be tailored by varying the nature of the incorporated bridging organic groups and these moieties may as-well be subsequently post-modified to introduce further functionalities. Numerous PMOs have been prepared using various bridging organic groups including methylene,[24] ethylene,[16,17] ethenylene,[25–29] phenylene,[20,30–32] thiophenylene,[33,34] biphenylene,[35] *etc.* under a wide range of pHs from highly basic to strongly acidic conditions. Consequently, PMO materials have been extensively studied because of the wide potential of application in catalysis, selective sorption, chromatography, sensing, optoelectronics, and host–guest chemistry.[22,23]

[a]*Center for Functional Nanomaterials, Department of Chemistry, KAIST, Daejeon, 305-701, Korea. E-mail: rryoo@kaist.ac.kr; Fax: +82-42-350-8130; Tel: +82-42-350-2830*
[b]*Graduate School of Nanoscience and Technology (WCU), KAIST, Daejeon, 305-701, Korea*
[c]*Canada Research Chair on Functional nanostructured materials, Department of Chemistry and Centre de recherche sur les matériaux avancés (CERMA), Université Laval, Québec, G1V 0A6, QC, Canada*
† Electronic supplementary information (ESI) available: ^{13}C CP NMR spectrum of KIT-6-(1)-100-E (Fig. S1) and XRD patterns for PMO samples synthesized under the presence or absence of butanol (Fig. S2). See DOI: 10.1039/c0jm01518k

Evidently, a highly interconnected organic-inorganic hybrid material combining the versatile properties of PMOs and the bicontinuous cubic $Ia\bar{3}d$ mesopore structure of KIT-6 could provide significant advantages in terms of molecular diffusion through the pore network, especially for processes involving bulky molecules, and supply enhanced host–guest interactions (*e.g.*, enhanced transport/contact *via* continuous channels and interfaces) as compared to corresponding 2-D hexagonal materials with one-dimensional channels.[30] However, to date there is only limited work reporting successful synthesis of cubic $Ia\bar{3}d$ PMO materials.[36,37] The first report described a synthesis of $Ia\bar{3}d$ PMO material based on applying the EISA[38] approach followed by a solvothermal post-treatment.[36] However, this synthesis of $Ia\bar{3}d$ PMO material had limitations, as it was achieved in a very narrow range of synthesis conditions (*i.e.*, reagent ratios and temperature) and is restricted to the formation of mesostructured thin films with only 1,2-bis(triethoxysilyl)ethane as the organosilica source. A later study discussed possible variation of the PMO hybrid mesostructure as a function of reagent ratios and surfactant packing parameters, including possible formation a cubic $Ia\bar{3}d$ mesophase.[37] However, this study focused on small pore PMO systems obtained using cationic gemini surfactants as structure-directing agents and bis(triethoxysilyl)ethane as the silicon source. Hence, developing an easier and more versatile synthesis of large pore periodic mesoporous organosilica (PMO) analogue to the KIT-6 material is still desired.

Herein, we propose a straightforward method to generate highly ordered cubic $Ia\bar{3}d$ phenylene-bridged PMOs in the $EO_{20}PO_{70}EO_{20}$-butanol-water system in high yields and high phase purity. Phenylene-bridged mesoporous organosilica material could be most attractive owing to the formation of molecular-scale periodicity in the pore walls, high functionality in further chemical modification, and high thermal stability ($\geq$500 °C).[30–32] Highly ordered 3-D cubic PMO materials, which are analogue to KIT-6 silica powders in terms of mesostructure, have thus successfully been prepared in aqueous acidic solutions by using a mixture of P123 ($EO_{20}PO_{70}EO_{20}$) triblock copolymer and n-butanol serving as dual structure-directing agents and 1,4-bis(triethoxysilyl)benzene as the organosilica source. The acid concentration and the reagent ratios were adjusted to allow for the formation of the bicontinuous cubic mesophase. The synthesis procedure is flexible and enables fine tuning of pore volume, specific surface area and mesopore size by simple variation of the hydrothermal aging temperature. Detailed characterization of the hybrid materials is provided by low and wide angle X-ray diffraction (XRD), transmission electron microscopy (TEM), solid state NMR and nitrogen physisorption analysis (at −196 °C) using modern non-local density functional theory (NLDFT) methods. This is the first report on the synthesis of well-ordered bicontinuous $Ia\bar{3}d$ large-pore cubic PMO materials exhibiting aromatic organic bridges in their framework walls.

Experimental

Syntheses

The KIT-6-type mesoporous organosilica materials were synthesized under acidic conditions using a mixture of poly(alkylene oxide)-based triblock copolymer Pluronic P123 ($EO_{20}PO_{70}EO_{20}$, Aldrich) and n-butanol (BuOH, Aldrich, 99.4%) as a structure-directing mixture. 1,4-bis(triethoxysilyl) benzene (BTEB, Aldrich, 96%) was used as the organosilica source. The molar composition of the starting reaction mixture was 0.034 P123/x HCl/y BTEB/z BuOH/400 H_2O, with (x = 0.25–2.0, y = 0.45–1.0 and z = 1.09–3.26). In a typical synthesis, 1.2 g of P123 was dissolved in 40.2 g of distilled water and 2.98 g of 2.0 M HCl solution with stirring at 35 °C. After complete dissolution, 1.08 g of BuOH was added at once. After 1 h stirring, 1.2 g of BTEB was added to the homogeneous clear solution. In that case, the molar ratio was 0.034 P123/1.0 HCl/0.5 BTEB/2.45 BuOH/400 H_2O. This mixture was left under vigorous stirring at 35 °C for 24 h. Subsequently, hydrothermal treatment of the reactant mixture was carried out at 100 °C for 72 h under static conditions in a closed polypropylene bottle. The white precipitate was then recovered by filtration, washed thoroughly with water, and dried at 100 °C in air overnight. Surfactant-free PMO materials was obtained by two consecutive solvent extractions as follows: 1.0 g of as-synthesized sample is stirred in 150 mL of ethanol with 3.8 g of 36% HCl aqueous solution at 60 °C for 6 h, filtered and dried at 100 °C in air. To ensure complete removal of the copolymer template, the PMO material samples were heated to 300 °C for 2 h under air flow. The samples obtained under these conditions are designated as PMO-KIT-6-(1)-100-E and PMO-KIT-6-(1)-100-T, for the material after copolymer-extraction by ethanol and the same material after subsequent thermal treatment at 300 °C, respectively. '100' refers to the temperature of hydrothermal reaction.

In another set of experiments, the hydrothermal treatment temperature, under static conditions, was varied from 80 to 130 °C for samples prepared with a reagent molar ratio of 0.034 P123/1.0 HCl/0.5 BTEB/2.59 BuOH/400 H_2O. The samples obtained with varying aging temperature are designated PMO-KIT-6-t, where t refers to the hydrothermal aging temperature. For comparison, a phenylene bridged PMO equivalent exhibiting 2-D hexagonal mesostructure was synthesized following the same procedure as described above, but in absence of BuOH. The molar composition of the starting reaction mixture for this sample was thus 0.034 P123/1.0 HCl/0.5 BTEB/0 BuOH/400 H_2O.

Characterization

Powder XRD patterns were recorded on a Rigaku Multiplex instrument using Cu-Kα radiation (λ = 0.15406 nm) operated at 40 kV and 40 mA (1.6 kW) in a step scan mode with narrow divergence slits. The nitrogen adsorption-desorption isotherms were measured at liquid nitrogen temperature (−196 °C) using a Quantachrome Autosorb-1MP volumetric adsorption analyzer. Samples were outgassed under vacuum for 12 h at 200 °C before the measurement. The Brunauer-Emmett-Teller (BET) equation was used to calculate the specific surface area from adsorption data obtained at P/P_0 between 0.05 and 0.2. The total volume was calculated from the amount of nitrogen adsorbed at P/P_0 = 0.95. The pore size distributions and cumulative pore volumes were determined by using NLDFT methods considering sorption of nitrogen at −196 °C in cylindrical silica pores.[39–41] Both the kernel of equilibrium NLDFT

isotherms (desorption branch), and the kernel of (metastable) NLDFT adsorption isotherms (adsorption branch) were applied for pore width determination.[42] For comparison, the pore size distributions were also calculated by analyzing the adsorption branch of the isotherm using the Barret-Joyner-Halenda (BJH) method. ^{29}Si MAS NMR and ^{13}C cross polarization (CP) MAS NMR spectra were obtained on a Bruker DSX400 spectrometer at room temperature with 7 mm zirconia rotor using resonance frequencies of 79.5 and 100.6 MHz for ^{29}Si MAS and ^{13}C CP MAS NMR, respectively. The ^{29}Si MAS NMR was operated at 5 kHz spinning rate, 15 s pulse delay and 4,000 scans. A typical spinning rate for ^{13}C CP NMR experiment was 4.5 kHz. 2 ms cross polarization contact time was used to acquire ^{13}C CP-MAS spectra with a repetition delay of 3 s and 10,000 scans. The chemical shifts for ^{29}Si and ^{13}C NMR spectra were referenced to tetramethylsilane. TEM images were taken from thin edges of particles supported on a porous carbon grid, using Philips F30 Tecnai equipment operated at 300 kV.

Results and discussion

Synthesis and characterization of mesoporous cubic *Ia*$\bar{3}$*d* phenylene-bridged PMO

The combination of P123 triblock copolymer ($EO_{20}PO_{70}EO_{20}$) dissolved in weakly acidic aqueous solution (0.14 M) in the presence of n-butanol and 1,4-bis(triethoxysilyl)benzene as a single organosilica source, enables facile synthesis of a well-defined 3-D cubic PMO material which should be viewed as organic-inorganic hybrid analogue of KIT-6 silica in terms of mesostructure and porosity. The bicontinuous *Ia*$\bar{3}$*d* mesostructure of this new large pore PMO material was demonstrated by the low angle powder XRD patterns measured for both the as-synthesized and the surfactant-free phenylene-bridged materials, PMO-KIT-6-(1)-100-E, as shown in Fig. 1. For the as-synthesized mesoporous benzene-silica sample, the XRD pattern indicates the characteristic diffraction peaks that can be assigned to the bicontinuous cubic structure (Fig. 1a). The unit cell parameter, *a* of the as-synthesized sample, as calculated from the (211) diffraction peak, is 24.1 nm. After template removal by solvent extraction in acidic ethanol, the diffraction peak intensities increase, as expected,[43] and the diffractogram exhibits up to seven well-resolved diffraction peaks which could clearly be indexed to the (211), (220), (321), (400), (420), (332) and (422) reflections of the bicontinuous cubic structure (space group *Ia*$\bar{3}$*d*). The unit cell parameter *a* of the PMO-KIT-6-(1)-100-E is calculated to be 23.2 nm, comparable to that obtained for the pure siliceous counterpart.[1,3,44]

The excellent 3-D cubic *Ia*$\bar{3}$*d* structure can further be evidenced by detailed TEM investigations. As illustrated in Fig. 2, representative TEM images viewed along various directions, *e.g.* [110], [111] and [531], clearly show extensive domains of cubic *Ia*$\bar{3}$*d* structure. The TEM images presented are consistent with the *Ia*$\bar{3}$*d* symmetry and uninterrupted channels are clearly viewed along the [111] zone axis corresponding to pores in projection. The material thus consists uniquely of large ordered domains of pure phase bicontinuous mesostructure. The respective Fourier diffractograms obtained from the TEM images confirm that the 3-D structure is commensurate with the cubic *Ia*$\bar{3}$*d* symmetry.[2,15,45–47] These data thus confirm that a highly ordered cubic *Ia*$\bar{3}$*d* mesostructured material is obtained by adding n-butanol to the present synthesis mixture at an adjusted HCl concentration.

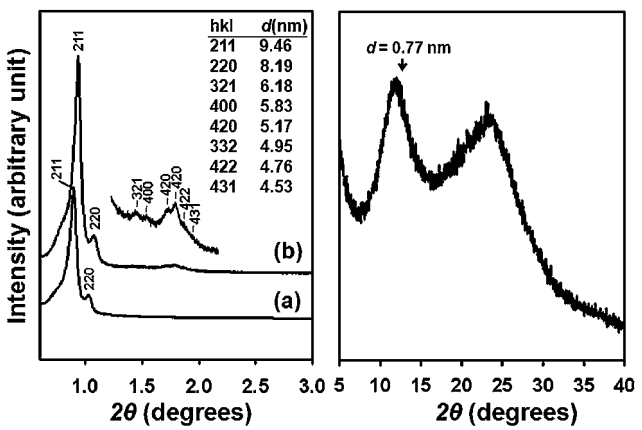

Fig. 1 (Left) Low angle powder XRD patterns for (a) as-synthesized and (b) surfactant-extracted cubic *Ia*$\bar{3}$*d* phenylene-bridged PMO material by ethanol, PMO-KIT-6-(1)-100-E. (Right) Wide-angle powder XRD pattern for PMO-KIT-6-(1)-100-E.

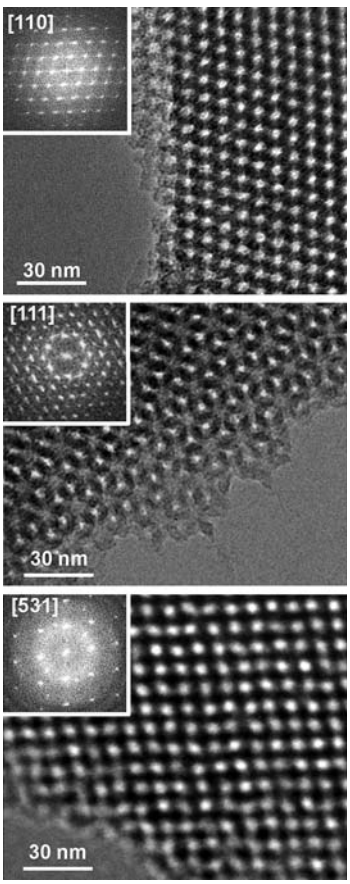

Fig. 2 TEM images of the cubic *Ia*$\bar{3}$*d* phenylene-bridged periodic mesoporous organosilica taken with the incident beam parallel to the [110], [111] and [531] directions. The insets are the corresponding Fourier diffractograms.

The presence of the organic moieties in the walls of the material was established by solid state NMR investigations. The ^{29}Si MAS NMR spectra for PMO-KIT-6-(1)-100-E and the corresponding sample after thermal treatment at 300 °C, PMO-KIT-6-(1)-100-T both show three signals at −61.4, −71.2, and −79.6 ppm corresponding to T^1 [$RSi(OSi)(OH)_2$], T^2 [$RSi(OSi)_2(OH)$], and T^3 [$RSi(OSi)_3$], respectively (Fig. 3a). The absence of signals due to Q^n [$Si(OSi)_n(OH)_{4-n}$] species between −90 and −120 ppm indicates that no carbon-silicon bonds were cleaved during the acidic synthesis and extraction step. The T^3/T^2 peak intensity ratios are about 0.50 and 0.63, for PMO-KIT-6-(1)-100-E and PMO-KIT-6-(1)-100-T, respectively. These values are much lower than those generally observed for mesoporous phenylene-silica prepared using alkyltrimethylammonium halide surfactants under alkaline conditions[20] but are well comparable with values obtained for similar materials derived from non-ionic surfactant (Brij-types)[31] or Pluronic copolymers,[48] considering the particularly low acid concentration used in our system.

The ^{13}C CP NMR spectrum (Fig. 3b) of PMO-KIT-6-(1)-100-T displays a strong signal at 132.6 ppm originating from the phenylene group connected to Si. For comparison, ESI Fig. S1† shows the ^{13}C CP NMR spectrum of PMO-KIT-6-(1)-100-E which was ethanol-washed, not thermally treated. In addition to the phenylene signal, additional peaks visible at about 16 ppm and 58 ppm are present which could most likely be attributed to non-hydrolyzed Si–O–CH_2CH_3 groups and/or surface ethoxy groups produced through the reaction with ethanol (*i.e.*, *transesterifcation* favored under acidic conditions).[49] Note that this ^{13}C NMR spectrum also indicates series of weak signals in the 50–75 ppm region which are generally attributed to residual P123 species.[50,51] If present, these residual fragments can be removed by performing an additional extraction step or by performing a thermal treatment at 300 °C[31,43,52] without affecting the $Ia\bar{3}d$ mesostructure or the aromatic moieties, phenylene bridges being stable up to 500 °C[20,30–32] (as demonstrated in Fig. 3b). The combination of ^{29}Si MAS and ^{13}C CP NMR analyses reveals that the framework of the PMO $Ia\bar{3}d$ material contains covalently bonded $O_{1.5}Si–C_6H_4–SiO_{1.5}$ units. These results are totally consistent with data obtained previously for 2-D hexagonal phenylene-bridged PMOs.[20,30–32,34]

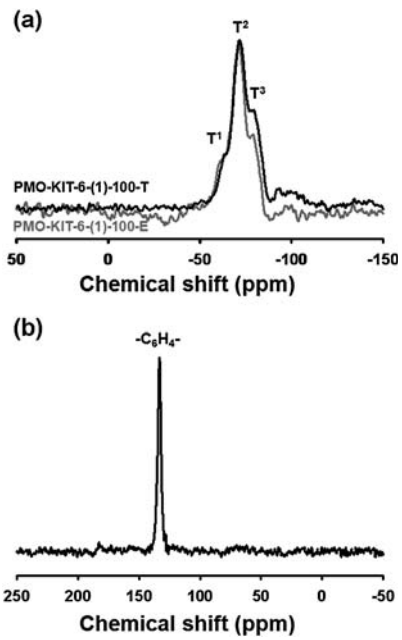

Fig. 3 (a) Solid state ^{29}Si MAS NMR spectra for the surfactant-free cubic $Ia\bar{3}d$ phenylene-bridged PMO materials, ethanol-washed PMO-KIT-6-(1)-100-E (gray) and thermally treated PMO-KIT-6-(1)-100-T (black) and (b) ^{13}C CP NMR spectrum for PMO-KIT-6-(1)-100-T.

Most importantly, Inagaki and coworkers reported the presence of a crystal-like wall structure in the case of phenylene-bridged PMOs with 2-D hexagonal mesopore structure which was synthesized under alkaline conditions.[20,53] For these materials, the molecular scale periodicity in the walls was confirmed both by wide-angle XRD investigations and high resolution TEM studies. From the XRD analyses, the authors observed periodic structures with spacing of 0.76 nm for 1,4-phenylene[20] and 1,3-phenylene[35] based PMO materials. Detailed TEM investigations conducted on these materials also revealed lattice fringes stacked along the channel axes, with uniform spacing distance of 0.76 nm and established that molecular-scale periodicity exists in the entire region of the pore walls. Similar crystal-like walls were further confirmed for other PMOs built on the basis of aromatic bridges templated by cationic alkylammonium halide surfactants under basic conditions.[35,54]

In the present case, the XRD data collected at wide angles for the phenylene-bridged KIT-6 PMO prepared under acidic conditions show the presence of only one broad signal with a spacing of 0.77 nm (instead of four peaks as observed by Inagaki *et al.*[20]). The observed distance $d = 0.77$ nm is in good agreement with the spacing of 0.76 nm reported by Inagaki *et al.*,[20] suggesting here somewhat similar periodic stacking of benzene ring layers in the pore walls with spacing of 0.77 nm. However, no other reflections correlated to this broad signal were observed at higher angles, which could be ascribed to limited short-range periodicity in the walls of the samples. TEM investigation could not reveal lattice fringes stacked along the channel axis. Previous reports on similarly prepared PMO materials indicated that formation of crystal-like walls could be difficult under acidic conditions using non ionic copolymers as structure-directing agents, because of weak interaction between surfactants and silica sources.[30–32,34] Wang *et al.*[55] observed only partial ordering of bridged benzene molecules in materials prepared under acidic conditions using non ionic Brij-type structure-directing agents, as concluded from TEM analyses (no XRD signals were reported).

In order to determine whether the observed limited molecular scale organization in the PMO-KIT-6 is a consequence of the gyroid framework structure, we also compared the wide angle XRD data of the cubic $Ia\bar{3}d$ PMO material with the wide angle XRD data obtained for a 2-D hexagonal equivalent prepared under similar experimental conditions except for the absence of n-BuOH in the *p6mm* case. The low angle and wide angle XRD patterns for 2-D hexagonal and 3-D cubic phenylene-bridged PMOs are depicted in Fig. S2.† Obviously, a relatively weak and broad signal is also observed in the case of the 2-D hexagonal phase, *i.e.* very small coherent scattering domains. Therefore, it is not possible to conclude that the lower crystalline organization in the walls of the cubic $Ia\bar{3}d$ PMO materials as compared to PMO materials obtained under alkaline conditions using ionic

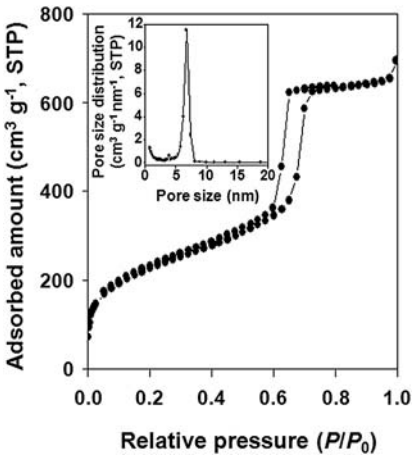

Fig. 4 Nitrogen adsorption-desorption isotherm measured at −196 °C for PMO-KIT-6-(1)-100-E. Inset shows the BJH pore size distribution obtained from the adsorption branch of the isotherm.

structure-directing agents[20,23] would be caused by the gyroid pore geometry. This is furthermore in line with previous observations of poor atomic order in the walls occurring in the case of PMOs prepared under acidic conditions exhibiting a comparatively fairly large wall thickness and arising from a silica/nonionic surfactant hybrid interface based on weak hydrogen bonding interactions.[30,31]

Mesoporosity was confirmed by nitrogen physisorption measurements performed at −196 °C. Fig. 4 shows the nitrogen adsorption-desorption isotherm and the corresponding BJH pore size distribution for PMO-KIT-6-(1)-100-E. The PMO material prepared by hydrothermal treatment at 100 °C for 72 h shows a typical type-IV isotherm with a sharp capillary condensation step at high relative pressures with H1-type hysteresis loop. These results are in good agreement with those of large-pore cubic $Ia\bar{3}d$ silica-based mesoporous analogues.[3] The pore size distribution is narrow, with a maximum at 6.8 nm as calculated by the BJH method applied to the adsorption branch of the isotherm. Note that this value seems to be slightly underestimated as compared to the pore width obtained using most accurate NLDFT method, *i.e.* 7.3 nm calculated using the NLDFT model of equilibrium isotherms (desorption branch). The choice of the NLDFT method for characterizing cubic $Ia\bar{3}d$ mesoporous materials will be commented on later in the paper. The surfactant-free mesoporous benzene-silica has a BET surface area of 818 $m^2 g^{-1}$ and a pore volume of 1.01 $cm^3 g^{-1}$. In addition, according to NLDFT cumulative pore volume data (not shown), a microporosity volume of 0.03 $cm^3 g^{-1}$ is observed for PMO-KIT-6-(1)-100-E. After the thermal treatment, the total pore volume remains almost constant (see Table 1) while the pore size is reduced by about 0.3 nm (NLDFT), consistent with a moderate contraction of the mesostructure occurring upon heating at 300 °C. In contrast, BET surface area is shown to increase substantially, as well as micropore volume, which could be consistent with a removal of undesired organic moieties from the framework walls (thus generating additional micropores).

Formation of the cubic $Ia\bar{3}d$ mesophase in the BTEB/P123/BuOH system

To substantiate the effects of the HCl concentration on the formation of mesostructure of the benzene-silica materials, different phenylene-bridged PMO materials were obtained with varying HCl concentrations and constant hydrothermal treatment conditions (100 °C for 72 h) with a fixed molar ratio of 0.034 P123/0.5 BTEB/2.72 BuOH/400 H_2O. From the evolution of the diffraction patterns presented in Fig. 5, we can see that the cubic $Ia\bar{3}d$ phase is formed in the presence of BuOH exclusively when the HCl concentration is decreased to as low as 0.14 M, with the other synthetic parameters remaining constant. Precisely, syntheses performed in the range 0.07–0.14 M HCl yield cubic $Ia\bar{3}d$ mesoporous benzene-silica materials. Higher (0.21 M) or lower (0.035 M) concentrations of acid catalyst result in the formation of poorly resolved mesophases (2-D hexagonal-like or wormhole-type). In the current $EO_{20}PO_{70}EO_{20}$-butanol-water system, we may thus speculate that slow hydrolysis and condensation of the organosilica precursors is desired to allow the formation of the gyroid structure in a similar way as observed before for the purely siliceous counterpart.[1,3]

It should be noted, however, that the optimized HCl concentrations in the range 0.07–0.14 M for the cubic $Ia\bar{3}d$ mesoporous benzene-silica materials is substantially lower than that

Table 1 Structural and physicochemical parameters determined (derived) from powder XRD and nitrogen physisorption measurements performed at −196 °C for the phenylene-bridged cubic $Ia\bar{3}d$ PMO samples obtained at different hydrothermal treatment temperatures

Samples	a^a/nm	$S_{BET}{}^b$/$m^2 g^{-1}$	$V_t{}^c$/$cm^3 g^{-1}$	$V_{mi\text{-}DFT}{}^d$/$cm^3 g^{-1}$	BJH_{ads}/nm	$NLDFT_{ads}{}^e$/nm	$NLDFT_{des}{}^f$/nm	$d_s{}^g$/nm
PMO-KIT-6-(1)-100-E	23.2	818	1.01	0.03	6.79	6.79	7.31	4.23
PMO-KIT-6-(1)-100-T	22.0	927	1.00	0.08	6.26	6.55	7.03	3.97
PMO-KIT-6-80	22.4	790	0.78	0.08	5.81	6.32	6.55	4.65
PMO-KIT-6-100	22.7	874	0.92	0.04	6.26	6.55	7.03	4.32
PMO-KIT-6-120	23.5	811	1.01	0.04	7.40	7.31	7.87	3.88
PMO-KIT-6-130	23.6	826	1.07	0.03	7.75	7.43	8.01	3.79

[a] a, unit cell parameter calculated as $6^{1/2}d_{211}$. [b] S_{BET}, apparent BET specific surface area deduced from the isotherm analysis in the relative pressure range from 0.05 to 0.20. [c] V_t, total pore volume taken at relative pressure $P/P_0 = 0.97$. [d] $V_{mi\text{-}DFT}$, micropore volume estimated using the NLDFT method. The model used for NLDFT evaluation was N_2 adsorbed on silica with cylindrical pores considering the adsorption branch (model of metastable adsorption). [e] $NLDFT_{ads}$, the primary mesopore diameter estimated using NLDFT method. The model used for NLDFT evaluation was N_2 adsorbed on silica with cylindrical pores considering the adsorption branch (model of metastable adsorption). [f] $NLDFT_{des}$, the primary mesopore diameter estimated using NLDFT method. The model used for NLDFT evaluation was N_2 adsorbed on silica with cylindrical pores considering the desorption branch (equilibrium sorption model). [g] d_s, wall thickness evaluated by a geometrical model: $d_s = a/2 - NLDFT_{des}$.[64]

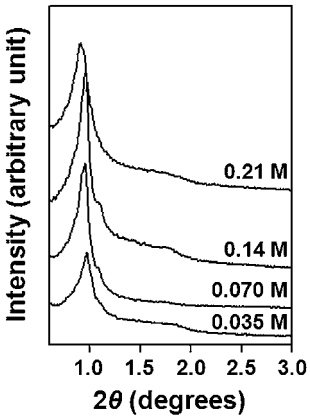

Fig. 5 Powder XRD patterns for phenylene-bridged PMO materials obtained using 0.034 P123/x HCl/0.5 BTEB/2.72 BuOH/400 H_2O. The molar ratio of HCl (x) was varied at $x = 0.25$, 0.50, 1.0, and 1.5, giving [HCl] = 0.035, 0.070, 0.14, and 0.21 M, respectively.

(0.25–0.75 M HCl) used in the case of the corresponding siliceous counterpart.[3] The organosilica source (BTEB) is believed to hydrolyze and condense faster than TEOS due to an inductive effect of the phenylene bridge and the resulting increase the density of the negative charges of the silicon and oxygen atoms (*i.e.*, this effect helps to decrease the activation energy of catalytic bond formation in between silicate ions, and the influence of bulky and rather hydrophobic character of BTEB is compensated by that inductive effect).[56] Slowing down the hydrolysis and condensation rates of BTEB by reducing significantly the HCl concentration in the system appears mandatory for enabling the co-surfactant species to tune efficiently the curvature of the micellar aggregates and thus direct the formation of the bi-continuous cubic mesophase permitted by slow condensation process.

Further experiments were conducted by varying the concentration of BuOH (z) from 1.09 to 3.26 with a molar ratio of 0.034 P123/1.0 HCl/0.5 BTEB/z BuOH/400 H_2O. The XRD patterns (Fig. 6a) recorded as a function of the BuOH amount show that, at a fixed amount of BTEB, the obtained mesostructure evolves from a 2-D hexagonal phase to the cubic $Ia\bar{3}d$ phase, finally to a disordered benzene-silica structure, while increasing the amount of butanol added to the synthesis mixture. Clearly, butanol is an additive indispensable in the formation of the cubic $Ia\bar{3}d$ mesostructure. In this system, BuOH is believed to act as a co-surfactant,[57,58] which co-micellizes together with the triblock block P123 micelles, controlling micellar interfacial curvature, similar to the case of the pure silica analogue.[1,3,59]

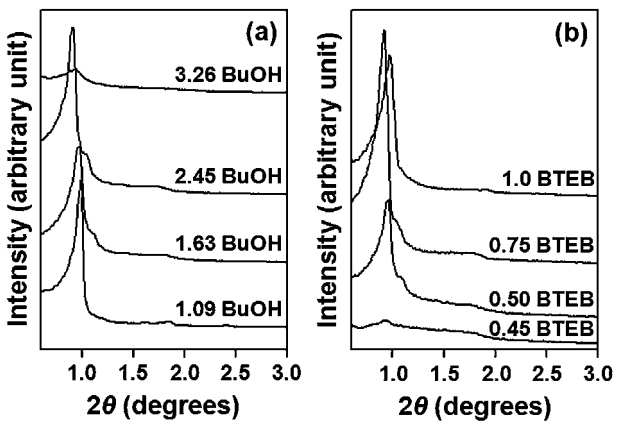

Fig. 6 (a) Powder XRD patterns for phenylene-bridged PMO materials obtained using 0.034 P123/1.0 HCl/0.5 BTEB/z BuOH/400 H_2O, with various molar ratios of BuOH (z). (b) Powder XRD patterns for phenylene-bridged PMO materials obtained using 0.034 P123/1.0 HCl/y BTEB/2.72 BuOH/400 H_2O, with various molar ratios of BTEB (y).

The role of benzene-silica precursor concentration in the formation of final mesoporous material was also studied in this $EO_{20}PO_{70}EO_{20}$-butanol-water system by using 0.034 P123/1.0 HCl/y BTEB/2.72 BuOH/400 H_2O, with varying BTEB molar ratios (y). As judged from the XRD patterns (Fig. 6b), highly ordered mesoporous benzene-silica with $Ia\bar{3}d$ structure can be prepared when the molar ratio of BTEB is fixed between 0.50 and 0.75. By increasing the molar ratio to 1.0, a 2-D hexagonal-like mesophase is formed. When the molar ratio of BTEB is decreased down to 0.45, only disordered mesophase was produced. We can thus assume that the formation mechanism for cubic $Ia\bar{3}d$ mesoporous PMO materials would be rather similar to that of the cubic $Ia\bar{3}d$ KIT-6 silica analogue.[1,3,59] In this case, the synthesis process would proceed similarly *via* a phase transition process which is function of the starting mixture composition, involving a modulated intermediate lamellar phase. Certain flexibility in the silicatropic-surfactant hybrid mesophase is required for the formation of the modulated lamellar phase (perforated lamellar) evolving then into the gyroid phase.[3,59] Higher concentration ($y \geq 1.0$) of BTEB usually increases condensation rate and produces less flexible organosilica oligomers that cannot allow for the change in curvature favored in *softer* frameworks. Thus, higher curvature 2-D hexagonal mesophase is generally formed. On the other hand, lower concentration of BTEB ($y \leq 0.45$) fails to provide sufficient benzene-silica building units to interact with the copolymer micellar surfaces, resulting in poorly ordered benzene-silica gels.

Porosity of the PMO-KIT-6 materials as a function of aging temperature

To tune textural parameters, the hydrothermal treatment temperature was varied between 80 and 130 °C for a given composition of 0.034 P123/1.0 HCl/0.5 BTEB/2.59 BuOH/400 H_2O. Aging time was 72 h in all cases. The XRD patterns of surfactant-free phenylene-bridged PMO samples obtained with different hydrothermal treatment temperatures are shown in Fig. 7. All of the samples show well-resolved diffraction peaks and the XRD patterns are characteristic of the $Ia\bar{3}d$ mesostructure, revealing that the high quality of resultant mesoporous materials is conserved. In addition, a gradual increase of the $d(211)$ value is observed with increasing aging temperature, reflecting progressive enlargement of the unit cell.

Fig. 8 shows the nitrogen adsorption-desorption isotherms and pore size distributions, respectively, for the same series of samples. For all of the samples prepared with different hydrothermal treatment temperature, steep capillary condensation steps are observed at high relative pressures ($P/P_0 = 0.6$–0.7), indicative of large cylindrical-like mesopores with fairly narrow

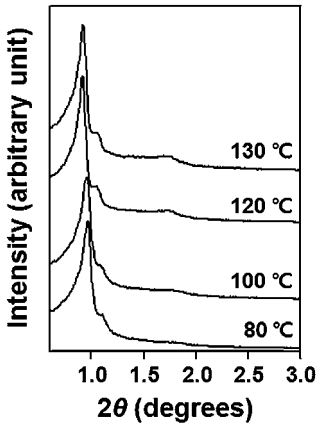

Fig. 7 Powder XRD patterns for phenylene-bridged PMO materials obtained using 0.034 P123/1.0 HCl/0.5 BTEB/2.59 BuOH/400 H_2O, at various temperatures of hydrothermal treatment (PMO-KIT-6-*x*, *x* refers to the temperature of hydrothermal treatment).

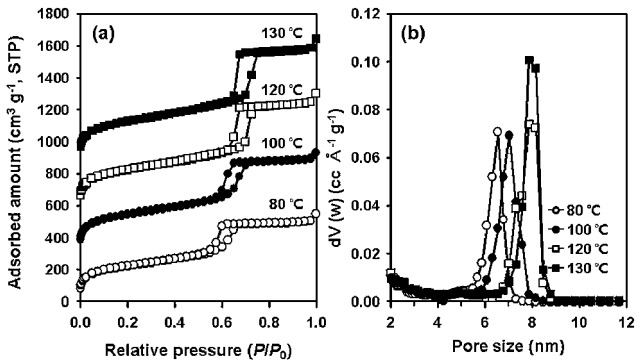

Fig. 8 (a) Nitrogen adsorption-desorption isotherms for surfactant-extracted PMO-KIT-6-*x* samples. The isotherms for PMO-KIT-6-100, PMO-KIT-6-120 and PMO-KIT-6-130 are offset by 300, 600 and 900 $cm^3\ g^{-1}$, respectively, for clarity. (b) NLDFT pore size distribution curves calculated from the isotherms shown in (a) (NLDFT equilibrium conditions - desorption branch).

size distribution. With increasing hydrothermal treatment temperature, an obvious shift of the hysteresis loop to higher relative pressures is observed (Fig. 8a), signifying that pore sizes are enlarged. Furthermore, the calculated NLDFT pore size distributions remain in all of the cases narrow as evidenced from the PSD plots depicted in Fig. 8b. Studies have demonstrated that modern NLDFT methods are most suitable to perform accurate pore size analysis of ordered mesoporous silica materials, *e.g.* MCM-41, SBA-15 silica, and the 3-D cubic MCM-48 and KIT-6 equivalents.[39–42,60,61] However, it was also revealed that the 3-D pore network structure in the cubic $Ia\bar{3}d$ materials could have a noticeable influence on the pore condensation and hysteresis behavior in these materials,[60,61] resulting in unexpected differences in NLDFT pore size values obtained from the adsorption and desorption branches. In the case of the hybrid PMO-KIT-6 materials described herein, a similar influence of the connected pore network on pore condensation and hysteresis behavior seems to be observed, *i.e.* the pore sizes obtained from NLDFT adsorption (isotherms of metastable adsorption) and those from NLDFT desorption (equilibrium isotherms) were not consistent (Table 1). The pore sizes obtained from the adsorption branch were slightly underestimated. In the case of KIT-6 silica, it was thus proposed that accurate pore size analysis of KIT-6 silica should be performed implementing the NLDFT equilibrium isotherm model (*i.e.*, using the desorption branch of the isotherms).[60] Accordingly, it is observed that the pore size of the cubic PMO materials increased from 6.5 to about 8.0 nm (Fig. 8b and Table 1) when the hydrothermal treatment temperature is increased from 80 to 130 °C. Note that the range of mesopore size control which could be achieved here is somewhat smaller than that obtained previously for the purely siliceous equivalent. A possibly lower flexibility in the hybrid mesophase (*i.e.*, more rigid framework walls) and longer aging time (3 days) applied here may account for this effect. Meanwhile, the pore volumes also increase from 0.78 to about 1.07 $cm^3\ g^{-1}$. This clearly evidences an unprecedented systematic control of the pore size of the large-pore cubic $Ia\bar{3}d$ PMO materials.

Micropore volumes could also be extracted from NLDFT cumulative pore volumes (adsorption branch), as listed in Table 1. In this series of samples, PMO-KIT-6-80 exhibits the highest micropore volume with 0.08 $cm^3\ g^{-1}$, a value that is consistent with micropore volumes obtained for purely siliceous copolymer-templated analogues.[10,60] However, in contrast to purely siliceous SBA-15 or KIT-6 materials, noticeable micropore volume is still detected (0.03 $cm^3\ g^{-1}$) for samples aged at elevated temperatures (> 120 °C).

Conclusion

A straightforward and versatile synthesis using n-butanol and triblock copolymer P123 ($EO_{20}PO_{70}EO_{20}$) as a structure-directing mixture and 1,4-bis(triethoxysilyl)benzene as the organosilica source was described to produce high quality large pore cubic $Ia\bar{3}d$ PMO materials. Importantly, both the addition of certain amount of butanol as a co-surfactant and low HCl concentrations (0.07–0.14 M in synthesis solution) are required to obtain a well-ordered cubic $Ia\bar{3}d$ mesophase. The wide angle XRD data revealed short range molecular-scale periodicity in the walls of the KIT-6-like PMO, most likely originated from regular arrangement of the bridging aromatic groups. However, in this acidic system based on triblock copolymer templating, molecular level ordering in the walls remained limited, in comparison with materials with thinner walls obtained under alkaline conditions using cationic surfactant.

This synthesis procedure also enabled an unprecedented fine tuning of pore volume, specific surface area and mesopore size by simple variation on the hydrothermal aging temperature. In terms of mesostructure ordering and textural properties, the hybrid large pore $Ia\bar{3}d$ PMO is quite similar to its pure silica counterpart, but the maximum pore size that could be achieved for the PMO materials seems to be limited to about 8 nm.

It could be expected that such materials exhibiting fully accessible 3-D channel structure consisting of an organic-inorganic hybrid framework will attract substantial interest for applications based on host–guest interactions where pore blockage could be a severe issue, *e.g.* adsorption/separation of biomolecules or liquid phase catalysis, and applications requiring extended and continuous interfaces between donor and acceptor

components, *e.g.* enhancing opto-electrical efficiency of occluded molecules, complexes, clusters or nanostructures.[62,63]

Acknowledgements

This work was supported by the Ministry of Education, Science and Technology in Korea (National Honor Scientist Program). Freddy Kleitz wishes to acknowledge financial support from NSERC and the Province of Québec (FQRNT).

Notes and references

1 F. Kleitz, S. H. Choi and R. Ryoo, *Chem. Commun.*, 2003, 2136.
2 Y. Sakamoto, T.-W. Kim, R. Ryoo and O. Terasaki, *Angew. Chem., Int. Ed.*, 2004, **43**, 5231.
3 T.-W. Kim, F. Kleitz, B. Paul and R. Ryoo, *J. Am. Chem. Soc.*, 2005, **127**, 7601.
4 J. Huang, G. Tian, H. Wang, L. Xu and Q. Kan, *J. Mol. Catal. A: Chem.*, 2007, **271**, 200; E. Li and V. Rudolph, *Energy Fuels*, 2008, **22**, 145; P. Handa, K. Holmberg, M. Sauthier, Y. Castanet and A. Mortreux, *Microporous Mesoporous Mater.*, 2008, **116**, 424; K. Soni, B. S. Rana, A. K. Sinha, A. Bhaumik, M. Nandi, M. Kumar and G. M. Dhar, *Appl. Catal., B*, 2009, **90**, 55; B. R. Jermy, D.-R. Cho, K. V. Bineesh, S.-Y. Kim and D.-W. Park, *Microporous Mesoporous Mater.*, 2008, **115**, 281; A. Prabhu, L. Kumaresan, M. Palanichamy and V. Murugesan, *Appl. Catal., A*, 2009, **360**, 59.
5 N. Calin, A. Galarneau, T. Cacciaguerra, R. Denoyel and F. Fajula, *C. R. Chim.*, 2010, **13**, 199; Y. Lü, G. Lu, Y. Wang, Y. Guo, Y. Guo, Z. Zhang, Y. Wang and X. Liu, *Adv. Funct. Mater.*, 2007, **17**, 2160.
6 B. Z. Tian, X. Liu, L. Solovyov, Z. Liu, H. Yang, Z. Zhang, S. Xie, F. Zhang, B. Tu, C. Yu, O. Terasaki and D. Zhao, *J. Am. Chem. Soc.*, 2004, **126**, 865; S. C. Laha and R. Ryoo, *Chem. Commun.*, 2003, 2138; F. Jiao, K. M. Shaju and P. G. Bruce, *Angew. Chem., Int. Ed.*, 2005, **44**, 6550; F. Jiao, A. Harrison, J. C. Jumas, A. V. Chadwick, W. Kockelmann and P. G. Bruce, *J. Am. Chem. Soc.*, 2006, **128**, 5468; A. H. Lu and F. Schüth, *Adv. Mater.*, 2006, **18**, 1793; F. Jiao, A. Harrison, A. H. Hill and P. G. Bruce, *Adv. Mater.*, 2007, **19**, 4063; Y. Shi, Y. Meng, D. Chen, S. Cheng, P. Chen, H. Yang, Y. Wan and D. Zhao, *Adv. Funct. Mater.*, 2006, **16**, 561; Y. Shi, Y. Wan, R. Liu, B. Tu and D. Zhao, *J. Am. Chem. Soc.*, 2007, **129**, 9522; H. Tüysüz, E. L. Salabas, C. Weidenthaler and F. Schüth, *J. Am. Chem. Soc.*, 2008, **130**, 280.
7 T. C. Wei and H. W. Hillhouse, *Langmuir*, 2007, **23**, 5689.
8 S. MacQuarrie, B. Nohair, J. H. Horton, S. Kaliaguine and C. M. Crudden, *J. Phys. Chem. C*, 2010, **114**, 57.
9 T. J. V. Yates, J. M. Thomas, J. J. Fernandez, O. Terasaki, R. Ryoo and P. A. Midgley, *Chem. Phys. Lett.*, 2006, **418**, 540.
10 A. Rumplecker, F. Kleitz, E. L. Salabas and F. Schüth, *Chem. Mater.*, 2007, **19**, 485.
11 H. Tüysüz, C. W. Lehmann, H. Bongard, R. Schmidt, B. Tesche and F. Schüth, *J. Am. Chem. Soc.*, 2008, **130**, 11510; T. W. Kim and L. A. Solovyov, *J. Mater. Chem.*, 2006, **16**, 1445.
12 V. Luzzati and P. A. Spegt, *Nature*, 1967, **215**, 701.
13 A. H. Schoen, *NASA Technical Note D-5541*; NASA, Washington, DC, 1970.
14 M. Clerc and E. Dubois-Violette, *J. Phys. II*, 1994, **4**, 275.
15 V. Alfredsson and M. W. Andersson, *Chem. Mater.*, 1996, **8**, 1141.
16 S. Inagaki, S. Guan, Y. Fukushima, T. Ohsuna and O. Terasaki, *J. Am. Chem. Soc.*, 1999, **121**, 9611.
17 B. J. Melde, B. T. Holland, C. F. Blanford and A. Stein, *Chem. Mater.*, 1999, **11**, 3302.
18 T. Asefa, M. J. MacLachlan, N. Coombs and G. A. Ozin, *Nature*, 1999, **402**, 867.
19 Y. Lu, H. Fan, N. Doke, D. A. Loy, R. A. Assink, D. A. LaVan and C. J. Brinker, *J. Am. Chem. Soc.*, 2000, **122**, 5258.
20 S. Inagaki, S. Guan, T. Ohsuna and O. Terasaki, *Nature*, 2002, **416**, 304.
21 B. Hatton, K. Landskron, W. Whitnall, D. Perovic and G. A. Ozin, *Acc. Chem. Res.*, 2005, **38**, 305.
22 W. J. Hunks and G. A. Ozin, *J. Mater. Chem.*, 2005, **15**, 3716.
23 F. Hoffmann, M. Cornelius, J. Morell and M. Fröba, *Angew. Chem., Int. Ed.*, 2006, **45**, 3216.
24 X. Y. Bao, X. Li and X. S. Zhao, *J. Phys. Chem. B*, 2006, **110**, 2656.
25 K. Nakajima, D. Lu, J. N. Kondo, I. Tomita, S. Inagaki, M. Hara, S. Hayashi and K. Domen, *Chem. Lett.*, 2003, **32**, 950.
26 W. Wang, S. Xie, W. Zhou and A. Sayari, *Chem. Mater.*, 2004, **16**, 1756.
27 Y. D. Xia, W. X. Wang and R. Mokaya, *J. Am. Chem. Soc.*, 2005, **127**, 790.
28 Y. D. Xia and R. Mokaya, *J. Mater. Chem.*, 2006, **16**, 395.
29 C. Vercaemst, P. E. de Jongh, J. D. Meeldijk, B. Goderis, F. Verpoort and P. van der Voort, *Chem. Commun.*, 2009, 4052; C. Vercaemst, M. Ide, H. Friedrich, K. P. de Jong, F. Verpoort and P. van der Voort, *J. Mater. Chem.*, 2009, **19**, 8839.
30 Y. Goto and S. Inagaki, *Chem. Commun.*, 2002, 2410.
31 M. P. Kapoor, N. Setoyama, Q. Yang, M. Ohashi and S. Inagaki, *Langmuir*, 2005, **21**, 443.
32 Y. Goto and S. Inagaki, *Microporous Mesoporous Mater.*, 2006, **89**, 103.
33 C. Y. Ishii, T. Asefa, N. Coombs, M. J. MacLachlan and G. A. Ozin, *Chem. Commun.*, 1999, 2539.
34 J. Morell, G. Wolter and M. Fröba, *Chem. Mater.*, 2005, **17**, 804.
35 M. P. Kapoor, Q. Yang and S. Inagaki, *J. Am. Chem. Soc.*, 2002, **124**, 15176.
36 Z. Zhang, X. Yan, B. Tian, S. Shen, D. Chen, G. Zhu, S. Qiu and D. Zhao, *Chem. Lett.*, 2005, **34**, 182.
37 H. I. Lee, C. Pak, S. H. Yi, J. K. Shon, S. S. Kim, B. G. So, H. Chang, J. E. Yie, Y. U. Kwon and J. M. Kim, *J. Mater. Chem.*, 2005, **15**, 4711.
38 C. J. Brinker, Y. Lu, A. Sellinger and H. Fan, *Adv. Mater.*, 1999, **11**, 579.
39 P. I. Ravikovitch and A. V. Neimark, *J. Phys. Chem. B*, 2001, **105**, 6817.
40 M. Thommes, in *Nanoporous Materials; Science and Engineering*, ed. G. Q. Lu and X. S. Zhao, Imperial College Press, London, U.K., 2004, pp. 317–364.
41 P. I. Ravikovitch and A. V. Neimark, *Langmuir*, 2000, **16**, 2419.
42 A. V. Neimark and P. I. Ravikovitch, *Microporous Mesoporous Mater.*, 2001, **44–45**, 697.
43 F. Kleitz, W. Schmidt and F. Schüth, *Microporous Mesoporous Mater.*, 2003, **65**, 1.
44 X. Liu, B. Tian, C. Yu, F. Gao, S. Xie, B. Tu, R. Che, L.-M. Peng and D. Y. Zhao, *Angew. Chem., Int. Ed.*, 2002, **41**, 3876; K. Flodström, V. Alfredsson and N. Källrot, *J. Am. Chem. Soc.*, 2003, **125**, 4402; Y. Q. Wang, C. M. Yang, B. Zibrowius, B. Spliethoff, M. Lindén and F. Schüth, *Chem. Mater.*, 2003, **15**, 5029.
45 A. E. Garcia-Bennett, O. Terasaki, S. Che and T. Tatsumi, *Chem. Mater.*, 2004, **16**, 813.
46 F. Kleitz, S. J. Thomson, Z. Liu, O. Terasaki and F. Schüth, *Chem. Mater.*, 2002, **14**, 4134.
47 M. Kaneda, T. Tsubakiyama, A. Carlsson, Y. Sakamoto, T. Ohsuna, O. Terasaki, S. H. Joo and R. Ryoo, *J. Phys. Chem. B*, 2002, **106**, 1256.
48 J. Morell, M. Gungerick, G. Wolter, J. Jiao, M. Hunger, P. J. Klar and M. Fröba, *J. Mater. Chem.*, 2006, **16**, 2809.
49 C. Lesaint, B. Lebeau, C. Marichal and J. Patarin, *Microporous Mesoporous Mater.*, 2005, **83**, 76.
50 C. M. Yang, B. Zibrowius, W. Schmidt and F. Schüth, *Chem. Mater.*, 2003, **15**, 3739; C. M. Yang, B. Zibrowius, W. Schmidt and F. Schüth, *Chem. Mater.*, 2004, **16**, 2918.
51 F. Bérubé, B. Nohair, F. Kleitz and S. Kaliaguine, *Chem. Mater.*, 2010, **22**, 1988.
52 F. Bérubé and S. Kaliaguine, *MicroporousMesoporous Mater.*, 2008, **115**, 469.
53 M. P. Kapoor, Q. Yang and S. Inagaki, *Chem. Mater.*, 2004, **16**, 1209.
54 J. Morell, C. V. Teixera, M. Cornelius, V. Rebbin, M. Tiemann, H. Amenitsch, M. Froba and M. Lindén, *Chem. Mater.*, 2004, **16**, 5564.
55 W. Wang, W. Zhou and A. Sayari, *Chem. Mater.*, 2003, **15**, 4886.
56 C. J. Brinker, *J. Non-Cryst. Solids*, 1988, **100**, 31.
57 P. Holmqvist, P. Alexandridis and B. Lindman, *Macromolecules*, 1997, **30**, 6788; P. Holmqvist, P. Alexandridis and B. Lindman, *J. Phys. Chem. B*, 1998, **102**, 1149.

58 F. Kleitz, T. W. Kim and R. Ryoo, *Langmuir*, 2006, **22**, 440.
59 S. Ruthstein, J. Schmidt, E. Kesselman, R. Popovitz-Biro, L. Omer, V. Frydman, Y. Talmon and D. Goldfarb, *Chem. Mater.*, 2008, **20**, 2779; S. Ruthstein and D. Goldfarb, *J. Phys. Chem. C*, 2008, **112**, 7102; L. Omer, S. Ruthstein, D. Goldfarb and Y. Talmon, *J. Am. Chem. Soc.*, 2009, **131**, 12466.
60 F. Kleitz, F. Bérubé, C. M. Yang and M. Thommes, *Stud. Surf. Sci. Catal.*, 2007, **170**, 1843; F. Kleitz, F. Bérubé, R. Guillet-Nicolas, C. M. Yang and M. Thommes, *J. Phys. Chem. C*, 2010, **114**, 9344.
61 M. Thommes, R. Köhn and M. Fröba, *Stud. Surf. Sci. Catal.*, 2002, **142**, 1695; M. Thommes, R. Köhn and M. Fröba, *Appl. Surf. Sci.*, 2002, **196**, 239; M. Thommes, R. Köhn and M. Fröba, *J. Phys. Chem. B*, 2000, **104**, 7932.
62 N. Mizoshita, Y. Goto, T. Tani and S. Inagaki, *Adv. Funct. Mater.*, 2008, **18**, 3699; N. Mizoshita, Y. Goto, T. Tani and S. Inagaki, *Adv. Mater.*, 2009, **21**, 4798.
63 V. N. Urade, T.-C. Wei, M. P. Tate, J. D. Kowalski and H. W. Hillhouse, *Chem. Mater.*, 2007, **19**, 768; Q. Guo, S. J. Kim, M. Kar, W. N. Shafarman, R. W. Birkmire, E. A. Stach, R. Agrawal and H. W. Hillhouse, *Nano Lett.*, 2008, **8**, 2982; Q. Guo, G. M. Ford, H. W. Hillhouse and R. Agrawal, *Nano Lett.*, 2009, **9**, 3060.
64 L. A. Solovyov, V. I. Zaikovskii, A. N. Shmakov, O. V. Belousov and R. Ryoo, *J. Phys. Chem. B*, 2002, **106**, 12198.